JANNAF Conference, December 1-5, 2003, Colorado Springs, CO

PORTABLE FLUORESCENCE IMAGING SYSTEM FOR HYPERSONIC FLOW FACILITIES

J.A. Wilkes
The College of William and Mary
Williamsburg, VA

D.W. Alderfer, S. B. Jones, and P.M. Danehy
NASA Langley Research Center
Hampton, VA

ABSTRACT

A portable fluorescence imaging system has been developed for use in NASA Langley's hypersonic wind tunnels. The system has been applied to a small-scale free jet flow. Two-dimensional images were taken of the flow out of a nozzle into a low-pressure test section using the portable planar laser-induced fluorescence system. Images were taken from the center of the jet at various test section pressures, showing the formation of a barrel shock at low pressures, transitioning to a turbulent jet at high pressures. A spanwise scan through the jet at constant pressure reveals the three-dimensional structure of the flow. Future capabilities of the system for making measurements in large-scale hypersonic wind tunnel facilities are discussed.

INTRODUCTION

The design and testing of the next generation of aerospace vehicles will rely increasingly on computer modeling through computational fluid dynamics, or CFD. While CFD has already become a powerful simulation tool, the equations at the heart of CFD often have many free parameters that need to be determined from experimental data in order to improve the predictive power of the technique. One means to acquiring this experimental data is through scalable testing carried out in hypersonic wind tunnel facilities. The flowfield variables of interest include temperature, pressure, velocity, and density, along with aerodynamic information like shock wave location, and laminar versus turbulent conditions.

Shadowgraph and schlieren are two-dimensional, path-averaged visualization techniques currently in use. Disadvantages of these techniques include lack of spatial resolution along the line-of-sight and insensitivity in regions of low pressure. Hot-wire anemometry and particle imaging velocimetry, or PIV,[1] are two techniques for measuring velocity that have been applied to supersonic flows. The hot-wire technique has a fast time response, but is limited to point measurements and is inherently intrusive. PIV requires seeding particles into the flow. Because particles are much larger and heavier than air molecules, particle paths may not always trace the true airflow or accurately reveal molecular flow structures. Furthermore, large-scale, long run-time facilities like those at NASA Langley create additional difficulties for particle seeding due to the large volumes of gas involved. Molecular-based techniques are the logical alternative in these large-scale facilities. Temperature measurements can be made using a non-intrusive technique like coherent anti-Stokes Raman spectroscopy (CARS).[2,3,4] Although this technique can provide single-shot temperature information, the measurements are also single-point. This means that gleaning three-dimensional temperature information can be time-consuming and that information from turbulent flows is necessarily averaged. Rayleigh scattering is another technique that has been used for temperature and density measurement in supersonic flows.[5] However, in low-density flows, the Rayleigh scattering signal strength is very low.

Planar laser-induced fluorescence (PLIF) represents an alternative to many of these techniques. Measurements using PLIF are two-dimensional, have sub-millimeter spatial resolution, and temporal resolution as low as 10 ns. Depending on the specifics of a given experiment, PLIF can be used for flow visualization, species mole fraction imaging, temperature mapping, or velocimetry. PLIF is a well-established technique, and others have demonstrated its usefulness in studying combustion in flame environments,[6] mapping temperature and velocity in laminar hypersonic flows in shock tunnels,[7] and studying separated flow regions in supersonic wind tunnels.[8,9] Several chemical species have been used as the probed species, the most common of which are acetone $((CH_3)_2CO)$,[10] the hydroxyl radical (OH),[11] iodine (I_2),[9,12] and nitric oxide (NO).[7,13] In the present investigation, we chose to use nitric oxide. Unlike OH, which is an intermediate product of combustion, NO is chemically stable and can be purchased in a gas bottle. Acetone is a liquid and iodine is a solid at room temperature and pressure; although both have a relatively high vapor pressure, seeding acetone or iodine into a large-volume gas flow is nevertheless challenging. Past investigations at NASA Langley have involved painting a small amount of iodine onto an aerospace model, allowing the iodine to be entrained into the flow.[9] Nitric oxide, in contrast, is a gas at room temperature and can be seeded locally or globally into a gas flow. It can also be naturally present in high-temperature or combusting flows. Because its molecular weight is nearly identical to air, NO molecules serve as reliable tracers of flow structures.

PLIF may also be able to provide data in regions of low pressure where other techniques break down. An advantage of probing nitric oxide is that its spectroscopy is very well understood. The primary mechanism working to decrease NO fluorescence signal in air, namely quenching by molecular oxygen, depends linearly on pressure, and is therefore less efficient at low pressures. Consequently, NO fluorescence works very well at low pressures whereas many other techniques, such as schlieren, shadowgraph, CARS and Rayleigh scattering, do not.

In order to use PLIF to make measurements in wind tunnel facilities, the entire system must be moved from the laboratory to the wind tunnel for the duration of the test, and then moved to another facility or back to the laboratory upon completion of the test. A disadvantage of the PLIF technique has been the amount of time and effort involved in moving and aligning all of the laser system components. In the present investigation, we have attempted to make the technique more functional by building a portable PLIF system, diagrammed in Fig. 1 and described in more detail below.

LASER-INDUCED FLUORESCENCE THEORY

Planar laser-induced fluorescence is a well-established technique, and only the details relevant to the present investigation will be discussed here. For a full description of PLIF theory, see references 13 and 14. In this application of PLIF, nitric oxide (NO) served as the probed species. A pulse of ultraviolet (UV) laser light excites NO molecules from their ground electronic state to their first excited electronic state. The wavelength of the laser is tunable between 224 nm and 227 nm, and as a result, particular vibrational and/or rotational transitions can also be induced depending on the specific wavelength selected. Excited NO molecules may experience collisions with other atoms or molecules. Such collisions may result in a change of the excited molecule's rotational quantum number (a process known as rotational energy transfer, or RET), or vibrational quantum number (vibrational energy transfer, or VET). Excited molecules may relax radiatively to their ground electronic state by emitting photons, a process known as fluorescence. The resulting fluorescence is broadband, coming not just from the laser-coupled excited state, but also from all states coupled through RET and VET. Additionally, excited molecules may relax non-radiatively by transferring their energy to other species present in the flow through collisions, a process known as quenching. Molecular oxygen (O_2) is the major quenching species of NO in air flows.[15] The intensity of the resulting fluorescence depends on the overlap integral of the laser lineshape and the absorption lineshape at the chosen wavelength. The absorption lineshape of NO at a particular wavelength depends on various line-broadening processes, including pressure, and on the Boltzmann fraction of the probed state,

2

which is a function of temperature. The requirements of a given test will dictate the criteria for the optimal laser wavelength.

For the initial application of PLIF using the portable system, we visualized an NO-seeded jet issuing into a low-pressure chamber. The laser was tuned to strongly-absorbing spectral lines, resulting in strong fluorescence relatively independent of temperature. In particular, a laser tuned to 226.256 nm (with a spectral linewidth of .002 nm) excited the Q_1+Q_{21} (N"=1), Q_1+Q_{21} (N"=2), and Q_1+Q_{21} (N"=3), rotational lines in the A(v'=0) $\leftarrow$ X(v"=0) transition. Scattered light and fluorescence at the laser's wavelength was blocked using spectral filters. Broadband fluorescence at wavelengths between 237 nm and 285 nm—corresponding to A(v'=0)$\rightarrow$X(v"=1-5) radiative transitions—was imaged at 90° to the laser sheet.

EXPERIMENTAL SETUP

PORTABLE SYSTEM DESIGN

The portable system comprises two 4 ft by 6 ft optical tables. A schematic of the portable system is presented in Fig. 1. The lower table has a recirculating chiller for a water-cooled intensified CCD (charge-coupled device) camera, dye circulators with a mixture of laser dyes [Rhodamine 590 and Rhodamine 610] in a methanol solvent, and an injection-seeded pulsed Nd:YAG laser [Spectra-Physics Quanta-Ray Pro-230-10; injection seeder Model 6350]. The Nd:YAG operates at 10 Hz and produces 1050 mJ per pulse at 1064 nm. This infrared
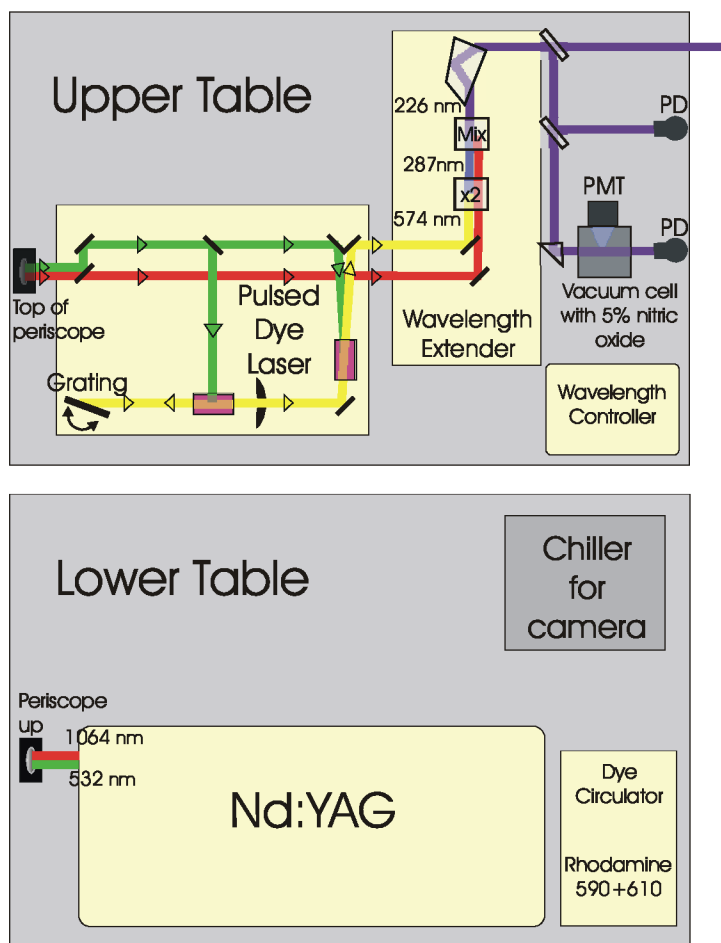

Figure 1. Schematic of portable system layout.

beam is then Type I frequency-doubled to produce 390 mJ of 532 nm in 10 ns pulses. When injection seeded, the spectral linewidth of the 1064 nm beam is approximately 3.4 x 10^{-4} nm (3 x 10^{-3} cm^{-1}). The residual 1064 nm pulses and the 532 nm pulses exit the Nd:YAG as collinear beams, which are then directed vertically through a beam pipe and through a hole in the upper table.

Once on the upper table, the beams enter a pulsed dye laser, or PDL [Spectra-Physics Quanta-Ray PDL-3]. A dichroic mirror separates the two beams. The 1064 nm beam passes straight through the PDL. The 532 nm beam pumps amplifier and oscillator dye cells. The laser dye circulating through the dye cells serves as the lasing medium for the PDL. An adjustable grating in the oscillator, controlled by an analog controller [QUESTEK 5220B] also located on the upper table, selects the lasing wavelength. The lasing wavelength of the PDL is broadly tunable. For the mixture of laser dyes used in this experiment and for output pulse energies greater than or equal to 90% of peak performance, this range is from 567nm to 577nm. By using the fifth order of the grating, the spectral linewidth of the resulting beam is approximately 2 x 10^{-3} nm (.07 cm^{-1}), according to the manufacturer.

After exiting the PDL, the 1064 nm beam and the yellow (~574 nm) beam enter a wavelength extender [Spectra-Physics Quanta-Ray WEX-1C]. The yellow beam is frequency-doubled to a wavelength of ~287 nm in the first crystal. By design, this wavelength is appropriate for exciting hydroxyl (OH). This extends the capabilities of the system to include OH PLIF, for combustion studies where OH is a more logical choice than NO as the probed species. For excitation of NO, the 287 nm beam is mixed with the 1064 nm beam in the second crystal of the WEX to produce 226 nm. The efficiency of doubling and mixing in the crystals of the WEX is a function of both wavelength and crystal angle. Consequently, the crystals must be rotated when the angle of the grating in the PDL (and therefore, its output wavelength) is changed. Although this can be done manually, the WEX has an electronic tracking feature, which uses a feedback loop to optimize the crystal angles to produce maximum beam intensity as the wavelength is scanned. The resulting beam has a central wavelength that is tunable from 224 nm to 227 nm with a measured spectral linewidth of 2 x 10^{-3} nm (0.4 cm^{-1}) and an energy of 3.5 mJ per pulse.

GAS CELL MONITORING SYSTEM

After exiting the WEX, a fraction of the beam is picked off by a quartz [UV-grade fused silica] window, creating a weak beam. A second such window directs a portion of this weak beam onto a white card (not shown), where it is viewed by a photodiode [Thorlabs, Inc. DET210], hereafter referred to as the laser photodiode. The laser photodiode is used to monitor changes in the laser's energy and correct data for any shot-to-shot fluctuations. The beam created by the first quartz window and transmitted through the second window is directed into a low-pressure gas cell. This gas cell has been evacuated and filled to 6 kPa with a 5% NO, 95% N_2 mixture. After passing through the gas cell, the beam terminates on a card (not shown), where it is viewed by a second photodiode, hereafter referred to as the absorption photodiode, which measures the intensity of light transmitted through the gas cell. Additionally, a photomultiplier tube, or PMT [Thorn EMI 9781B], is mounted to the gas cell at 90° to the beam propagation direction. A filter [Schott UG5 Filter Glass] in front of the PMT blocks out scatter at the laser's wavelength. In addition, a neutral density filter [ND 1] in front of the PMT reduces the incident light intensity by 90% so that the voltage supplied to the PMT (in the present work, −600 V) can be of sufficient magnitude so as to ensure that it is operating in a linear response regime.

When the laser is tuned to an allowed optical transition in NO, the beam is partially absorbed and then reemitted as broadband fluorescence by the NO in the cell. The absorption photodiode then measures a corresponding decrease in the light transmitted through the gas cell, while the PMT measures the relative intensity of the resulting fluorescence. If the laser wavelength is then detuned from the absorptive transition, the NO in the cell will no longer absorb the beam, the absorption photodiode will register an increase in transmitted intensity, and the PMT will register a decrease in fluorescence intensity. These data can be recorded and normalized for fluctuations in laser intensity by the readings from the laser photodiode. In this

4

manner, the laser can be scanned over a range of wavelengths and NO fluorescence and transmission spectra can be recorded. This gas cell monitoring system allows the system operator to ensure that the laser is initially tuned to the selected transition in NO, and that it remains tuned to that transition during the course of a measurement.

SHEET-FORMING AND POSITIONING OPTICS

The majority of the UV beam leaving the WEX passes through a hole in the end panel of the enclosed laser cart. Upon exiting the laser cart, the beam is directed through sheet-forming lenses and into the test section by a series of turning prisms. The first lens is a converging cylindrical lens with a focal length of 72 mm, which causes the beam to focus and then diverge in one dimension. The second lens is a spherical lens with a focal length of 1 m, which collimates the beam in the first dimension and loosely focuses it in the other dimension. The focal point of the laser sheet was positioned approximately 15 mm above the imaged region. The result is a 74 mm wide by ~0.5 mm thick laser sheet in the measurement region. The thickness of the laser sheet is the limiting factor in determining the system's spanwise (out-of-plane) spatial resolution. A motorized translation stage [Velmex single axis BISLIDE Tandem Positioning System] allows the spanwise position of the laser sheet to be adjusted in increments of 0.005 mm.

FLUORESCENCE IMAGING SYSTEM

Broadband fluorescence from the measurement region is imaged by an intensified CCD [Princeton Instruments ICCD-576 G/B THX]. A filter [Schott UG5 Filter Glass] in front of the camera blocks out most of the light at the laser's wavelength. Data acquisition and storage is controlled via software [Princeton Instruments WinView, Version 1.6.2]. A recessed window on the side of the test section allows the camera to be as close as possible (67 cm) to the imaged region. A [105 mm focal length, UV-Nikkor] camera lens images a 26.8 mm x 17.9 mm region of the flow through an image intensifier onto a 192 pixel x 128 pixel region of the CCD array, a spatial resolution of ~0.14 mm x 0.14 mm (7.2 pixels/mm); together, the imaging optics and the size of the CCD array represent the limiting factors in determining the in-plane spatial resolution of the imaging system. The camera has a thermoelectric cooler, which cools the detector to -30°C and is in turn cooled by chilled recirculating water. This cooling system requires that the camera be continually purged by dry nitrogen to prevent condensation. The intensifier is gated by a high-voltage pulse generator [Princeton Instruments PG-200] capable of creating camera gate widths as short as 10 ns. For the present work, the gate width was increased to 1000 ns to capture the maximum fluorescence possible; the fluorescence lifetime of NO under these conditions was ~220 ns. The intensifier gate width is the limiting factor in determining the technique's temporal resolution.

ELECTRONIC COMPONENTS

Electronic components for controlling data acquisition and coordinating the timing of other components of the PLIF system are mounted on a portable rack, located near the laser cart. Outputs from the laser photodiode, absorption photodiode, and PMT are passed through a gated integrator and boxcar averager [SRS Model 280]. A customized LabVIEW program running on a rack-mounted computer allows fluorescence and transmission spectra to be acquired, sending signals to the wavelength controller of the PDL to vary the laser's wavelength and recording the outputs of the photodiodes and PMT through the integrator. Timing of the firing of the laser lamps and Q-switch and the camera intensifier gate is controlled through a trigger tiger [LabSmith Programmable Experiment Controller LC880; "trigger," Version 5.02 software]. The rack also houses the camera controller [Princeton Instruments ST-130] and pulse generator [Princeton Instruments PG-200] as well as the high-voltage power supply for the PMT.

5

FACILITY CONSIDERATIONS

The results presented in this paper were obtained after installing the system in the 15-inch Mach 6 wind tunnel facility at the NASA Langley Research Center. A schematic of the experimental layout is presented in Fig. 2 and a photograph of the system as installed in the wind tunnel facility is presented in Fig. 3. The enclosed laser cart is positioned to allow tunnel operators to open and close the door to the test section as required. The laser sheet enters the test section through a window on the top of the test section. The motorized translation stage mounted above the tunnel allows the laser sheet to be scanned spanwise across the test section. This can be done either between tunnel runs or during a run, depending on the region of interest within the flow. Recessed windows on the side of the test section allow the intensified CCD cameras to be as close as possible to the measurement region while they image the fluorescence. As an added safety precaution, the movement of the translation stage, the timing of data acquisition by the cameras, and the nitric oxide flow rate have all been made remotely controllable via trigger switches located in the wind tunnel control room.
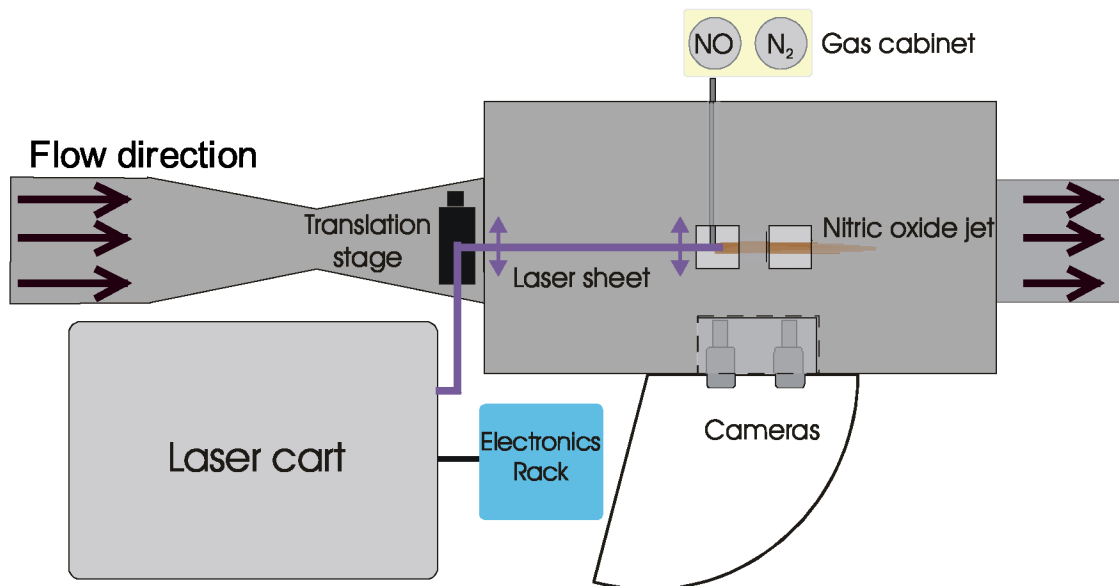

Figure 2. Schematic of the experimental layout in the 15-inch Mach 6 wind tunnel facility. An arc marks the path of the test section door. Flow direction is from left to right.

Nitric oxide was chosen as the probe species for the reasons described above. Because NO is not naturally present in this facility, it must be seeded into the flow either locally or globally. The main disadvantage of using NO is that it is toxic and corrosive, and many safety precautions had to be incorporated into the NO plumbing system. A forced-ventilation gas cabinet [Matheson Tri-Gas] houses a bottle of a 5% NO, 95% N_2 gas mixture. Toxic gas detectors [Crowcon Detection Instruments, Ltd.] located in the gas cabinet and on the side of the laser cart set off audible and visible alarms when NO concentrations above 25 ppm are detected (25 ppm is the time-weighted average maximum permissible exposure level for an 8 hour work day determined to be safe by OSHA standards). The gas cabinet includes a pneumatic valve designed to shut off the NO supply if either detector measures 25 ppm, if the ventilation for the gas cabinet fails, or if an excessive flow rate of NO is measured. The gas cabinet also houses a bottle of nitrogen, which can be used both to dilute the NO mixture being seeded into the test section, and to purge all plumbing lines of NO at the end of a test.

Figure 3. Photograph of the laser cart and electronics rack installed in the 15-inch Mach 6 wind tunnel facility. The test section is visible behind the electronics rack. Arrows indicate the path of the laser beam.

SPECTRAL SCANS

In order to verify the operation of the laser system and to ensure that the laser was tuned to the correct wavelength, spectral scans were obtained using the gas cell monitoring system described above. Measurements from the absorption photodiode and the PMT were normalized by the laser energy measured from the laser photodiode to correct for fluctuations in laser intensity. The resulting spectra are displayed in Fig. 4 and Fig. 5. In Fig. 4, the top graph shows the measured normalized fluorescence (red) and transmission (dark blue) spectra. The bottom graph shows calculated[16] theoretical fluorescence (orange) and transmission (light blue) spectra. In Fig. 5, measured and calculated spectra are plotted together on the same graph and displayed for two smaller regions of the spectrum. The upper graph shows portions of the $R_1 + R_{21}$, S_{21}, $Q_1 + Q_{21}$, and R_2 bands while the lower graph shows the O_{12} band head. Rotational quantum numbers label the individual spectral lines.

The theoretical fluorescence spectra in Fig. 4 and Fig. 5 were calculated using a spectral simulation software program[16]. These spectra were generated for room temperature (295 K), with the theoretical laser linewidth fitted to the spectral linewidth measured from the experimental spectrum (2×10^{-3} nm). A qualitative theoretical absorption spectrum was generated by using the calculated theoretical fluorescence spectrum and the Beer-Lambert law: $I = I_0 e^{-\alpha c L}$. Here, I is the calculated transmitted intensity, $\alpha = \alpha(\lambda_{laser})$ is the effective absorption coefficient of NO as a function of the laser's wavelength λ_{laser}, c is the effective concentration, and L is the measured path length through the gas cell. The value of the intensity of the calculated fluorescence spectrum was substituted for $\alpha(\lambda_{laser})$ at each value of the laser's wavelength. This assumes that the transition is not being saturated by excessive laser power, but rather, that fluorescence and absorption are related linearly. Finally, I_0 and c were fitted to match the magnitude of the measured absorption spectrum.
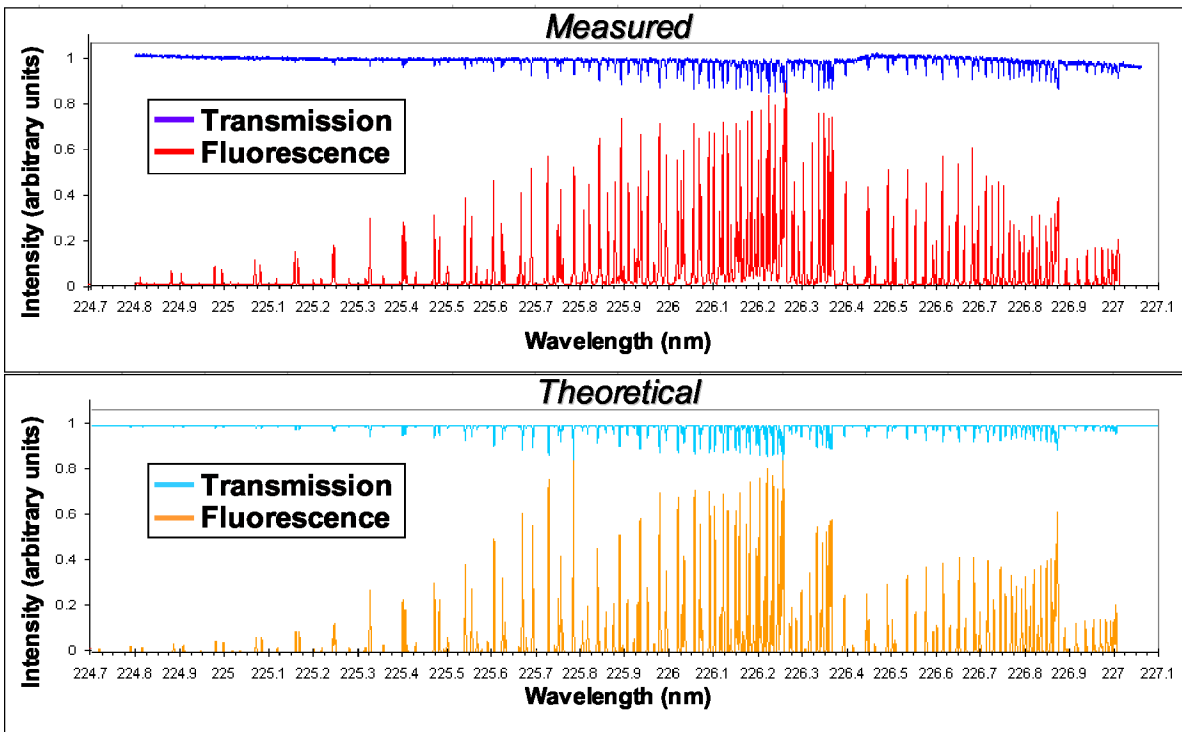
7

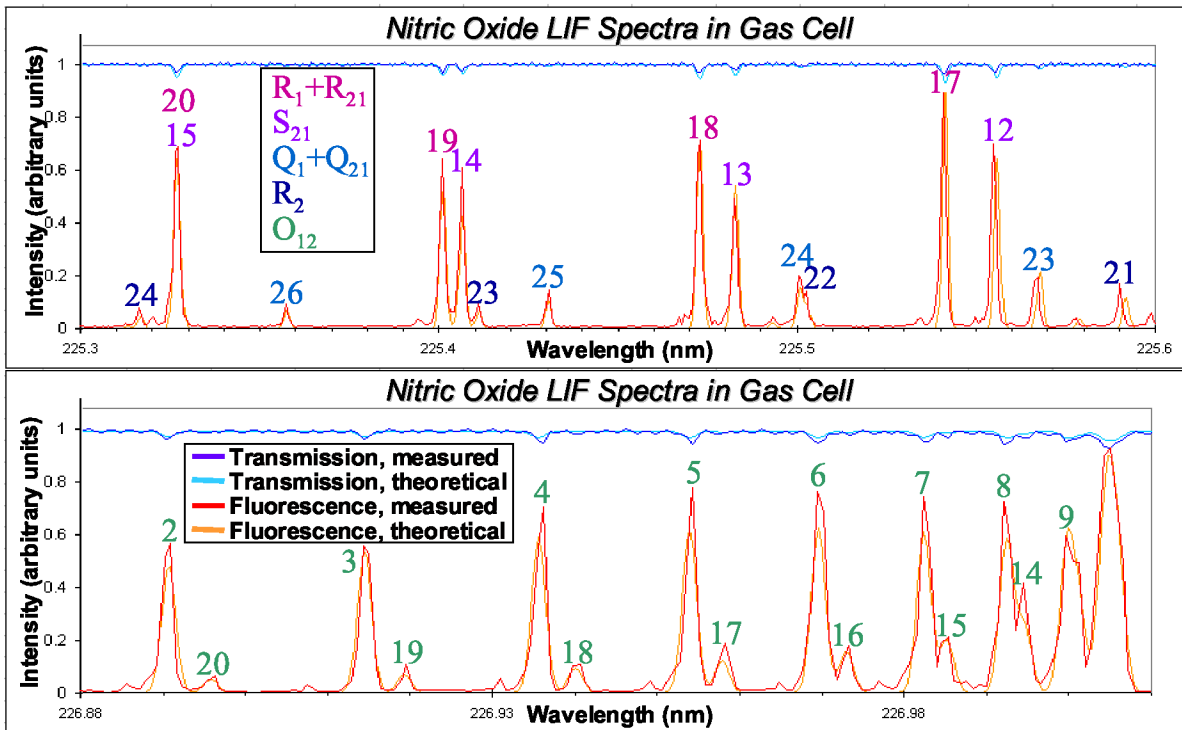Figure 4. Measured and calculated transmission and fluorescence spectra for nitric oxide.

Figure 5. Two smaller regions of the nitric oxide spectrum. Rotational quantum numbers label the individual spectral lines.

RESULTS AND DISCUSSION

IMAGING OF A FREE JET

        In this initial demonstration of the PLIF measurement system, the wind tunnel was not operated. Rather, the wind tunnel test section was pumped down to a near-vacuum (0.2 – 7 kPa). A relatively high-pressure mixture of NO and N_2 was plumbed into the test section and through a 0.83 mm inside diameter nozzle. Pressures just upstream of the nozzle were not measured; the pressures specified below are estimated. Owing largely to the low levels of molecular oxygen (O_2) and to the low pressure, quenching was negligible and the signal levels in the resulting images were very high. For test section pressures of more than ~6 kPa, the resulting flow was a subsonic turbulent jet. For test section pressures of less than ~6 kPa, the resulting flow was a supersonic underexpanded jet, characterized by barrel shock and Mach disk flow structures. Selected images from these tests are displayed in Fig. 6-8.

        The series of images in Fig. 6 show single shot images taken with the laser sheet positioned at the center of the nozzle flow. For this series of images, the test section pressure was held relatively constant at ~7 kPa; pressure upstream of the nozzle was estimated to be ~170 kPa, corresponding to a 3 slpm flow rate of a 5% NO / 95% N_2 mixture. The resulting flow is that of a turbulent subsonic jet. The last image shown is a 44-shot average. Camera gain was set to 4.
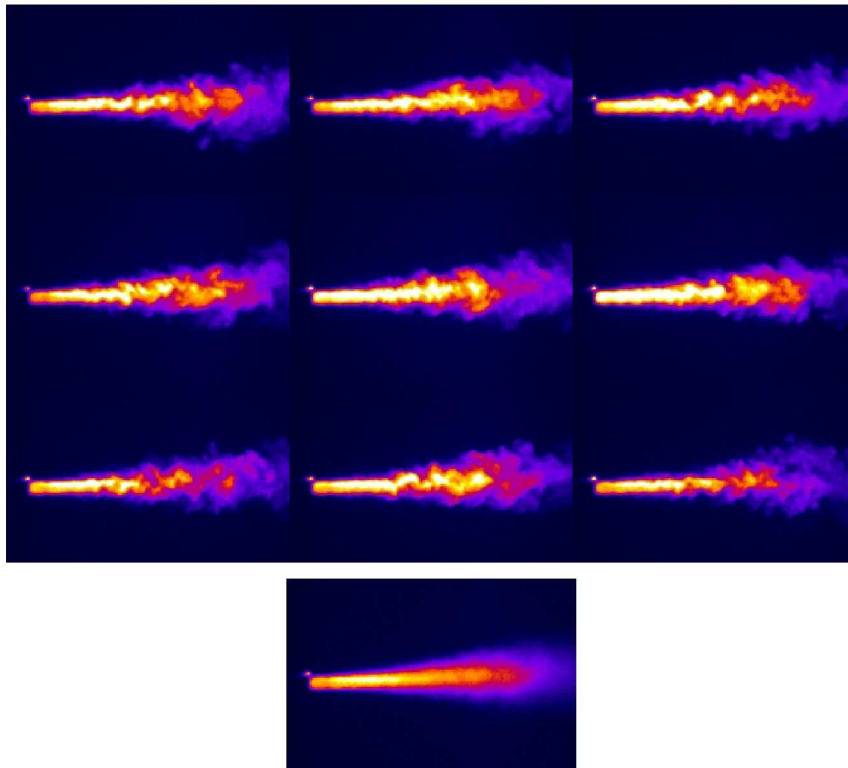

Figure 6. Nine single-shot images and one averaged image from the center of a subsonic turbulent jet exhausting through a 0.83 mm nozzle into a chamber at relatively high pressure. Each image is 27 mm across.

        The series of images in Fig. 7 were taken with the laser sheet positioned in the center of the nozzle flow. Test section pressure was slowly increased from 0.8 kPa to 5.2 kPa. For these and all subsequent images, the estimated pressure upstream of the nozzle was 550 kPa and the flow out of the nozzle was a ~1% NO / ~99% N_2 mixture. As the test section pressure increases, the size of the barrel shock can be seen to decrease. Camera gain was set to 3.
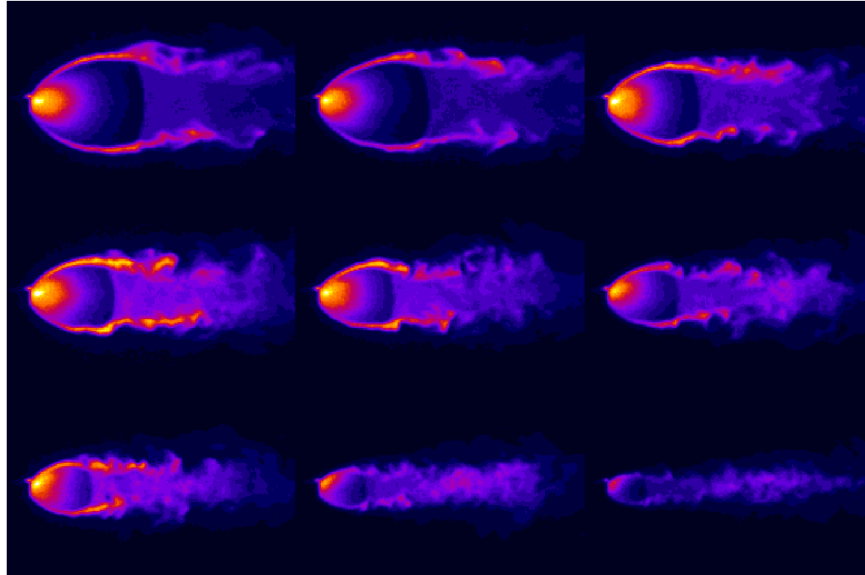
Figure 7. Single-shot images from the center of a supersonic underexpanded jet, exhausting into a low-pressure chamber. Test section pressure has been continuously increased from the first image to the last.

For the series of images in Fig. 8, the test section was held at a relatively constant pressure of ~0.8 kPa. The laser sheet was then scanned spanwise through the flow at a constant rate of 0.1 mm/s. Turbulent flow structures that appear to be streamwise vortex tubes can be seen outside of the barrel shock in several of the images. Camera gain was set to 4.
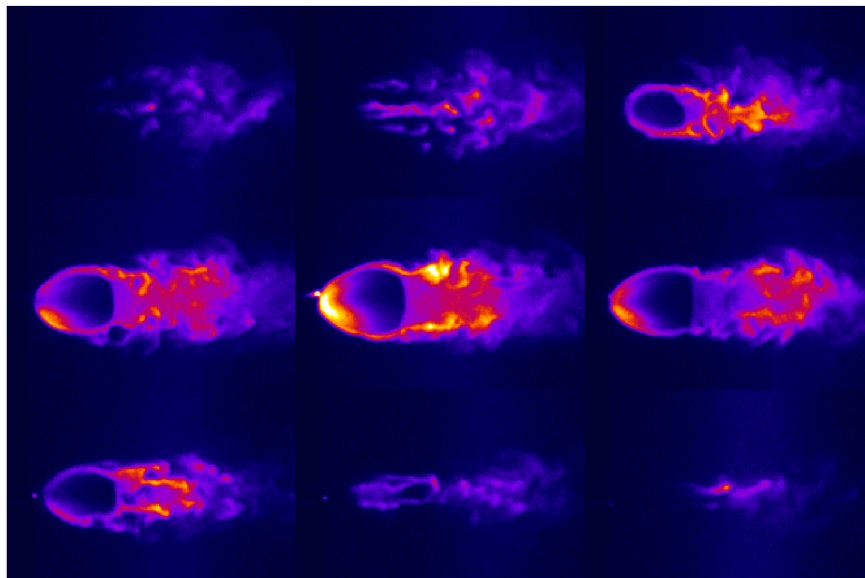

Figure 8. Single-shot images taken from an out-of-plane scan through a supersonic underexpanded jet, exhausting into a low-pressure chamber at constant pressure.

In Fig. 9, the pressure in the test section was held relatively constant at an even lower pressure of ~0.3 kPa, resulting in a large barrel shock. The laser sheet was again scanned spanwise through the jet, this time at a constant rate of 0.15 mm/s. Turbulent flow structures that appear to be vortex tubes located on the outside of the barrel shock are once again visible in several of the images. The resulting series of images demonstrates the capability of the system to resolve small (~0.5 mm) three-dimensional flow structures.
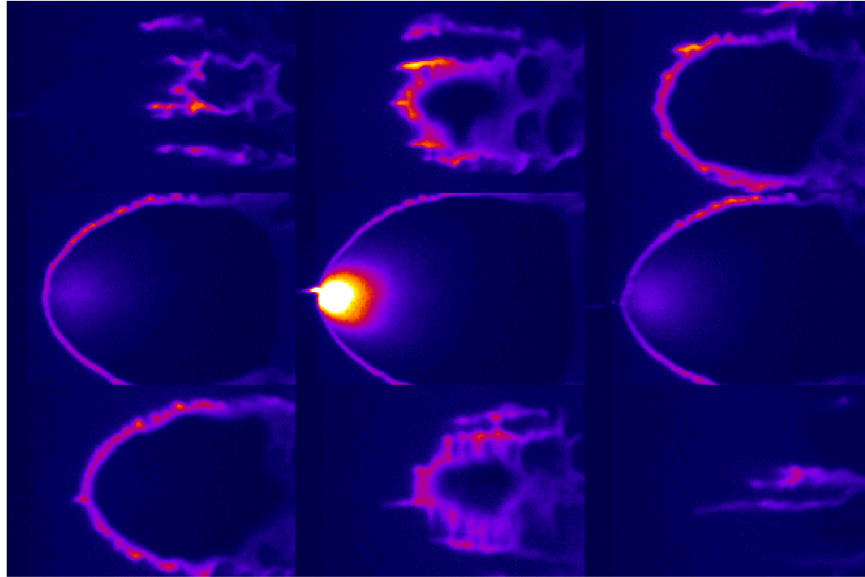
Figure 9. Single-shot images taken from an out-of-plane scan through a supersonic underexpanded jet, exhausting into a very low-pressure chamber at constant pressure. Note the streamwise vortex tubes visible on the outer edges of the flow.

One of the strengths of the PLIF technique is the ability to provide data in low-pressure environments. The widely used schlieren technique provides crisp, high-contrast images at higher pressures, but loses contrast in low-pressure regions. As a demonstration of the advantages of using PLIF for flow visualization in low-pressure regions, two schlieren images of the free jet are presented in Fig. 10.
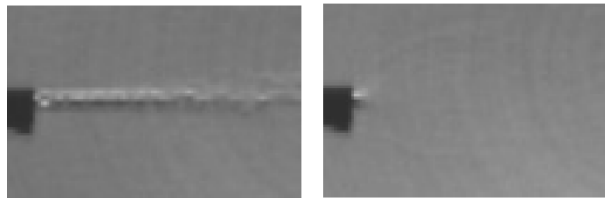

Figure 10. Schlieren images of a turbulent subsonic jet and a supersonic underexpanded jet. Conditions were the same as those in Fig. 6 and Fig. 8, respectively.

The test section pressure was ~7 kPa in the first image, and ~0.8 kPa in the second image, corresponding to the same conditions as Fig. 6 and Fig. 8 above. At the higher pressures in the first image, the turbulent jet is clearly visible, although turbulent flow structures cannot be resolved due to the low sensitivity of the technique. In the second image, the lower pressure and three-dimensional nature of this flow yield an image where flow structures are only faintly distinguishable. The faint concentric arcs visible in both images are due to distortions caused by imperfections in the test section windows, which were of lower quality than those normally used for schlieren imaging. By contrast, these same features are clearly distinguishable in the images acquired using PLIF, as shown in Fig. 6 and Fig. 8, respectively. The low quality of schlieren image in low-pressure flow regions is a common problem in hypersonic wind tunnel testing. The NO PLIF technique should allow more satisfactory visualization in these low-pressure flowfields.

CONCLUSIONS

We have successfully constructed a portable PLIF system designed to make measurements in hypersonic wind tunnel facilities. As a first demonstration of the flow visualization capability of the system, images were acquired of an NO-seeded free-jet flow. These images reveal several advantages of the NO PLIF technique. The first is the ability to

resolve turbulent flow structures, which are masked by path-averaged and time-averaged techniques. The second is the ability to visualize flow in low-pressure regions, where other techniques suffer from low signal or low contrast. The third is the capacity to make three-dimensional measurements by scanning the laser sheet through the flow. These features demonstrate the potentially powerful tool of NO PLIF flow-visualization. Demonstrations of the system's capacity for velocimetry and thermometry are planned for the near future. Ultimately, the portability and versatility of this system will represent a significant addition to the tools available to researchers making measurements in large-scale hypersonic wind tunnel facilities.

ACKNOWLEDGMENTS

REFERENCES

1. Beresh, S.J., Clemens, N.T., and Dolling, D.S. *Relationship between upstream turbulent boundary-layer velocity fluctuations and separation shock unsteadiness* AIAA Journal, Vol.40, No.12, 2412-22, (Dec 2002).

2. Cutler, A. D., Danehy, P. M., Springer, R. R., O'Byrne, S., Capriotti, D. P., and DeLoach, R., *CARS thermometry in a supersonic combustor for CFD code validation*, AIAA Journal, in press.

3. Grisch, F., Bouchardy, P., Pealat, M., Chanetz, B., Pot, T., and Coet, M. C., *Rotational temperature and density measurements in a hypersonic flow by dual-line CARS*, App. Phys. B B56, 14-20 (1993).

4. Boyce, R.R., Pulford, D.R.N., Houwing, A.F.P., and Mundt, C., *Rotational and vibrational temperature measurements using CARS in a hypervelocity shock layer flow and comparisons with CFD calculations*, Shock Waves Journal, Vol. 6, 41-45 (1996).

5. Panda, J., and Seasholtz, R.G., *Measurements of shock structure and shock-vortex interaction in underexpanded jets using Rayleigh scattering*, Phys. Fluids, Vol. 11, 3761-3777 (1999).

6. Seitzman, J. M., Kychakoff, F., and Hanson, R. K., *Instantaneous temperature field measurements using planar laser-induced fluorescence*, Optics Letters, Vol. 10, No. 9, 439-441 (Sep 1985).

7. O'Byrne, S., Danehy, P. M., and Houwing, A. F. P., *Nonintrusive temperature and velocity measurements in a hypersonic nozzle flow*, AIAA Paper 2002-2917 (2002).

8. Lachney, E. R., and Clemens, N. T., *PLIF imaging of mean temperature and pressure in a supersonic bluff wake*, Experiments in Fluids, Vol. 24, 354-363 (1998).

9. Exton, R. J., Balla, R. J., Shirinzadeh, B., Hillard, M. E., and Brauckmann, G. J., *Flow visualization using fluorescence from locally seeded I_2 excited by an ArF excimer laser*, Experiments in Fluids, Vol. 26 335-339 (1999).

10. Thurber, M. C., Grisch, F., and Hanson, R. K., *Temperature imaging with single- and dual-wavelength acetone planar laser-induced fluorescence*, Optics Letters, Vol. 22, No. 4, 251-253 (Feb 15, 1997).

11. Carter, C. D., and Laurendeau, N. M., *Wide- and narrow-band saturated fluorescence measurements of hydroxyl concentration in premixed flames from 1 bar to 10 bar*, Applied Physics B (Lasers and Optics), Vol. B58, No.6, 519-28 (June 1994).

12. Donohue, J. M., and McDaniel, J. C., Jr., *Computer-controlled multiparameter flowfield measurements using planar laser-induced iodine fluorescence*, AIAA Journal, Vol. 34, No. 8, 1604-1611 (Aug 1996).

13. Paul, P. H., Lee, M. P., and Hanson, R. K., *Molecular velocity imaging of supersonic flows using pulsed planar laser-induced fluorescence of NO*, Optics Letters, Vol. 14, No. 9, 417-419 (May 1, 1989).

14. Eckbreth, A. C., *Laser Diagnostics for Combustion Temperature and Species, 2nd ed.*, Gordon and Breach Publishers, The Netherlands (Oct 1996).

15. Paul, P. H., Gray, J. A., and Durant, J. L., Jr., *Collisional quenching corrections for laser-induced fluorescence measurements of NO $A^2\Sigma^+$*, AIAA Journal, Vol. 32, No. 8 (Aug 1994).

16. Luque, J., and Crosley, D. R., *LIFBASE: Database and Spectral Simulation Program (Version 1.5)*, SRI International Report MP 99-009 (1999).